Origin of Superlinear Power Dependence of Reaction Rates in Plasmon-Driven Photocatalysis: A Case Study of Reductive Nitrothiophenol Coupling Reactions

Kexun Chen and Hui Wang*

Department of Chemistry and Biochemistry, University of South Carolina, Columbia, South Carolina 29208, United States

* Corresponding author.

Email: wang344@mailbox.sc.edu; Phone: 1-803-777-2203; orcid.org/0000-0002-1874-5137.

ABSTRACT

The superlinear dependence of reaction rate on the power of excitation light, which may arise from both thermal and nonthermal effects, has been a hallmark of plasmon-driven photocatalysis on nanostructured metal surfaces. However, it remains challenging to distinguish and quantify the thermal and nonthermal effects because even slight uncertainties in measuring the local temperatures at the active surface sites may lead to significant errors in assessing thermal and nonthermal contributions to the overall reaction rates. Here we employ surface-enhanced Raman scattering as a surface-sensitive *in situ* spectroscopic tool to correlate detailed kinetic features of plasmon-mediated molecular transformations to the local temperatures at the active sites on photocatalyst surfaces. Our spectroscopic results clearly reveal that the superlinearity in the power dependence of reaction rate observed in a plasmon-driven model reaction, specifically the reductive coupling of *para*-nitrothiophenol adsorbates on Ag nanoparticle surfaces, originates essentially from photothermal heating rather than nonthermal plasmonic effects.

KEYWORDS: plasmonic photocatalysis, power dependence, photothermal transduction, hot electrons, Raman thermometry, surface-enhanced Raman scattering

Plasmon-driven photocatalysis has emerged as a paradigm-shifting approach toward the solar-tochemical energy conversion, enabling us to harness nanoscale light-matter interactions as a unique leverage to kinetically modulate interfacial molecular transformations on nanostructured metal surfaces with selectively controlled reaction outcomes.¹⁻¹² Unambiguous elucidation of detailed mechanisms underpinning plasmonic photocatalysis, however, has often been challenging due to strong interplay among multiple plasmon-derived nonthermal and thermal effects over a broad distribution of timescales.^{2, 7, 10, 12, 13} A widely adopted experimental strategy for mechanistic studies involves exploration of the relationship between the reaction rate and the excitation power, which delivers highly informative messages concerning the underlying reaction mechanisms.^{1, 3, 14-17} The rates of plasmon-driven photocatalytic reactions have been observed to be linearly proportional to the excitation power under moderate continuous wave (CW) illumination but may switch to a superlinear dependence when the excitation power exceeds certain threshold values or under illumination by pulsed lasers due to multiphoton absorption^{1, 3, 14, 17} and plasmon-induced activation energy reduction.^{15, 18, 19} Such superlinear power dependence is a unique feature of plasmonic photocatalysis, 1, 14, 17 fundamentally distinct from the sublinear power dependence commonly observed in conventional semiconductor-based photocatalysis. Another singular characteristic of plasmon-driven photocatalysis is that the reaction rate increases exponentially with the working temperature, whereas the rate of a semiconductor-driven photocatalytic reaction typically goes down at elevated temperatures. 1, 11, 12, 17 Whether the superlinearity of power dependence observed in plasmon-driven photocatalysis originates primarily from the hot carrier-related nonthermal effects or the plasmonic photothermal heating has been a vigorously debated open question well-worthy of indepth investigations. 7, 11, 16, 19-23

It remains an immensely challenging task to fully distinguish and precisely quantify the thermal and nonthermal contributions to the kinetic enhancement of plasmon-mediated photochemical reactions because of the difficulties in accurately measuring the local temperatures at the adsorbate-

occupying active surface sites under operando conditions.^{7, 11, 13, 24, 25} The local temperatures on the surfaces of light-illuminated photocatalysts, however, vary drastically from site to site, deviating substantially from the apparent bulk temperatures in the photocatalysts and the surrounding media, which can be measured straightforwardly using thermocouples or thermal cameras. Here we measure the local surface temperatures in the plasmonic hot spots on light-illuminated nanostructured metal surfaces through surface-enhanced Raman spectroscopy (SERS)-based nanothermometry. We also utilize SERS as an *in situ* molecular fingerprinting tool to precisely monitor the plasmon-driven transformations of molecular adsorbates residing in the hot spots. Combination of SERS-based thermometric and kinetic measurements enables us to correlate the molecule-transforming kinetics to the local temperatures at the active sites on photocatalyst surfaces.

We assembled quasi-spherical Ag nanoparticles (45 ± 4 nm in diameter) coated with monolayers of thiolated molecular adsorbates into hexagonally close-packed nanoparticle arrays on Si substrates with sub-10 nm interparticle gaps (Figure 1A) over areas typically on the order of $\sim 10^3$ - 10^4 μm^2 (Figure S1 in the Supporting Information). The as-assembled Ag nanoparticle arrays exhibited unique triple functionalities, serving as SERS substrates, photothermal transducers, and plasmonic photocatalysts simultaneously. The strong plasmon coupling among neighboring Ag nanoparticles gave rise to a broad light extinction peak across the visible and near-infrared spectral regions (Figure S2 in the Supporting Information). ²⁶ Upon optical excitation of the plasmons by a near-infrared laser (785 nm), the local electric fields were enormously enhanced in the interparticle gaps, which functioned as the hot spots for Raman enhancement. We used SERS to monitor the structural evolution of molecular adsorbates in these hot spots during plasmonic photothermal heating and photocatalytic reactions. In our SERS measurements, a homebuilt reaction chamber²⁶⁻²⁹ assembled on top of the Si-supported Ag nanoparticle arrays was filled with either ambient air or an aqueous solution of 2 mM K₂CO₃ (pH = 9) and a CW laser (785 nm) was focused onto a focal spot about 2 um in size on the samples using a confocal Raman microscope. Our SERS-based thermometry involved the use of chemisorbed thiophenol (TP) as a molecular probe with SERS features that are intrinsically sensitive to the change of temperatures. As shown in Figure 1B, the relative SERS intensity of the ring scissoring mode (β_{CC} , 1000 cm⁻¹) decreased significantly with respect to that of the C-S stretching mode (v_{CS} , 1072 cm⁻¹) after thermal treatment at an elevated temperature due to thermally induced irreversible conformational changes.^{27, 30} Similar SERS spectral changes upon temperature elevation were also previously observed in surface-adsorbed TP molecules on a variety of other Ag nanostructures.^{27, 28, 30}

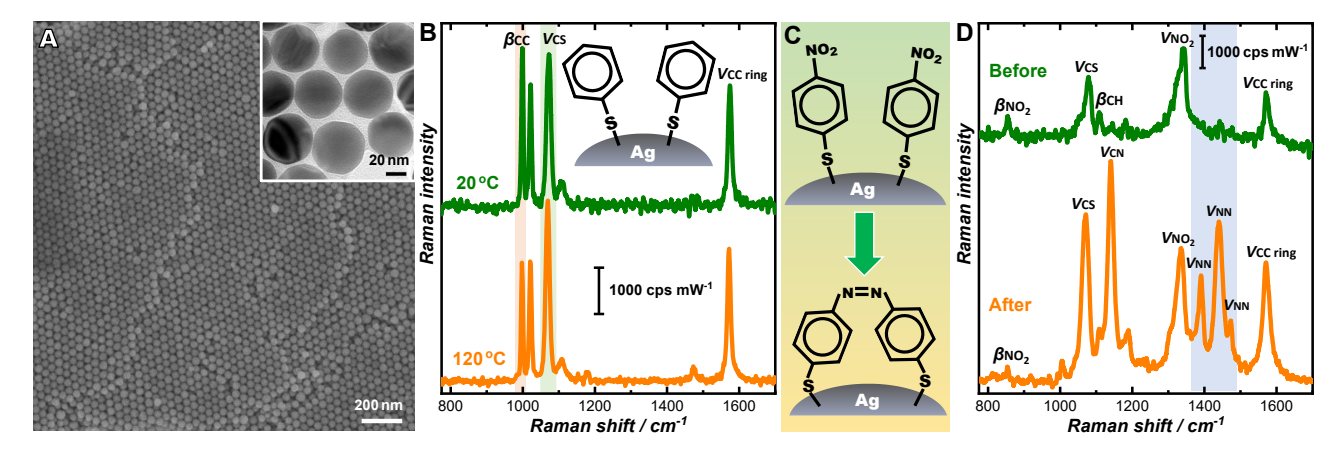


Figure 1. (A) SEM image of Ag nanoparticle arrays on a Si substrate. The inset shows a TEM image of Ag nanoparticles. (B) SERS spectra of TP on Ag nanoparticle arrays collected at 20 °C and after treating the sample at 120 °C for 30 min. (C) Schematic illustration of the reductive coupling of pNTP, which produces DMAB. (D) SERS spectra of pNTP on Ag nanoparticle arrays before and after laser illumination at a P_{ex} of 0.97 mW in air for 20 s. The SERS spectra shown in panels B and D were collected at 20 °C at a P_{ex} of 0.08 mW with an integration time of 5 s.

The photocatalytic reaction we focused on in this work was the plasmon-driven reductive coupling of *para*-nitrothiophenol (pNTP) on Ag nanoparticle surfaces, through which an aromatic azo compound, p,p'-dimercaptoazobenzene (DMAB), was produced (Figure 1C). The pNTP-to-DMAB conversion could be precisely monitored by SERS because pNTP and DMAB exhibited strikingly different SERS features (Figure 1D). pNTP molecules chemisorbed to Ag nanoparticle surfaces exhibited a set of characteristic SERS peaks, including the benzene ring mode ($v_{CC ring}$, 1572 cm⁻¹), the nitro stretching mode (v_{NO2} , 1334 cm⁻¹), the C-S stretching mode (v_{CS} , 1072 cm⁻¹), the nitro

scissoring mode (β_{NO2} , 856 cm⁻¹), and the C-H bending mode (β_{CH} , 1105 cm⁻¹).³¹ After laser illumination, the relative intensities of the ν_{NO2} and β_{NO2} modes decreased with respect to that of the $\nu_{CC ring}$ mode, while the spectral signatures of DMAB, including the azo stretching modes (ν_{NN} , 1480, 1438, and 1393 cm⁻¹) and the C-N stretching mode (ν_{CN} , 1146 cm⁻¹),^{31, 32} became clearly resolved. Although the reductive coupling of pNTP has been a plasmonic hot electron-driven model reaction intensively investigated over the past decade,^{27, 31, 33-49} strikingly opposing claims have been made in the literature regarding the relative contributions of photothermal heating and nonthermal plasmonic effects.^{36, 42, 45, 48} Here we endeavor to clarify this controversy through combined thermometric and kinetic measurements using SERS as a spectroscopic tool.

The empirical parameter, Q, which was defined as the intensity ratio between the β_{CC} mode at 1000 cm⁻¹ and the v_{CS} mode at 1072 cm⁻¹ in the SERS spectra of TP, kept decreasing as the bulk temperature of the surroundings progressively increased over a broad range from 20 °C up to ~120 °C (Figure 2A). At temperatures higher than 140 °C, however, the SERS signals dropped drastically due to thermally induced surface melting of the Ag nanoparticles and decomposition of the molecular adsorbates. Within the temperature range of 20-120 °C, a linear relationship between Q and temperature was clearly observed (Figure 2B), which provided a calibration curve for our SERSbased nanothermometry. After the samples were exposed to continuous laser illumination for 2 min, a thermal equilibrium between photothermal transduction and heat dissipation was fully established, and Q reached its steady state value, Q_{ss} , accordingly. The relationships between Q_{ss} and the excitation power, P_{ex} , for the chemisorbed TP molecules exposed to air and an aqueous medium were shown in Figure S3 in the Supporting Information. Based on the measured Q_{ss} values, we were able to further calculate the steady-state temperature, T_{ss} , using the calibration curve shown in Figure 2B. In our case, T_{ss} represented the apparent steady-state temperature averaged over all hot spots within the focal volume of the excitation laser rather than the local temperature inside an individual hot spot. As shown in Figure 2C, higher T_{ss} values were achieved in air than in the aqueous medium at identical P_{ex} s because the thermal conductivity of water ($\sim 0.60 \text{ W m}^{-1} \text{ K}^{-1}$) was 24 times higher than that of air (0.025 W m⁻¹ K⁻¹). Our observations were fully in line with the local plasmonic heating effects in a tip-enhanced Raman scattering system.⁵⁰ T_{ss} increased with P_{ex} and exhibited a sublinear P_{ex} -dependence, which could be fitted using the following quadratic polynomial function:²⁰

$$T_{ss} = T_0 + aP_{ex} - bP_{ex}^2$$
 (Equation 1),

in which a and b are two coefficients describing the linear and nonlinear thermal responses of the plasmonic photocatalysts, respectively, and T_0 is the ambient temperature in dark, which is 20 °C in our case. Both a and b exhibited significantly lower values in water than in air essentially due to the different heat dissipation rates in these two media. Under moderate light excitations, a linear relationship between T_{ss} and P_{ex} was typically observed because the contribution of the nonlinear response term was negligibly small in comparison to the linear response term. However, at sufficiently high P_{ex} , the nonlinear term became more pronounced due to modification of the materials' permittivity, frequency shift of plasmon resonances, decreased quality factor of plasmonic cavity, and changes in the thermal properties of the interfaces and local environment. Although the excitation powers investigated in this work was in the sub-mW to mW range, the power densities in the focal plane were on the order of 10^3 - 10^4 W cm⁻², significantly higher than those typically used in plasmonic photocatalysis. Although the resonance of T_{ss} was observed in our case.

To study the kinetics of photothermal heating, we tracked the temporal evolutions of Q under continuous laser illumination at various P_{ex} s both in air and in the aqueous environment through time-resolved SERS measurements until the thermal equilibrium was fully established (Figure S4 in the Supporting Information). The elevation of local temperature in the hot spots also led to slight spectral downshifts (within ~ 4 cm⁻¹) and intensity increase of the v_{CS} and the $v_{CC ring}$ modes (Figure S5 in the Supporting Information), in line with our previous observations on TP-coated Ag nanocubes.²⁷ As

shown in Figure 2D and 2E, the temporal evolutions of the apparent local temperature, T, in the hot spots could be well-described by the following first-order rate law:

$$T = (T_{ss} - T_0)(1 - e^{-k_T t})$$
 (Equation 2),

where t is the illumination time and k_T is the apparent rate constant for temperature elevation, which describes the net kinetic outcome of photothermal transduction and heat dissipation. The values of k_T and T_{ss} at various P_{ex} s extracted from curve-fitting are shown in Figure 2F and 2G, respectively. Both k_T and T_{ss} increased with P_{ex} , and superlinear relationships between k_T and P_{ex} were clearly observed. When switching the surrounding medium from air to an aqueous solution, both k_T and T_{ss} decreased significantly. Due to the complications caused by surface adsorbates, Si substrates, and interparticle interactions, the heat generation and dissipation processes were believed to be significantly more sophisticated than those of an individual nanoparticle dispersed in a homogeneous dielectric medium.

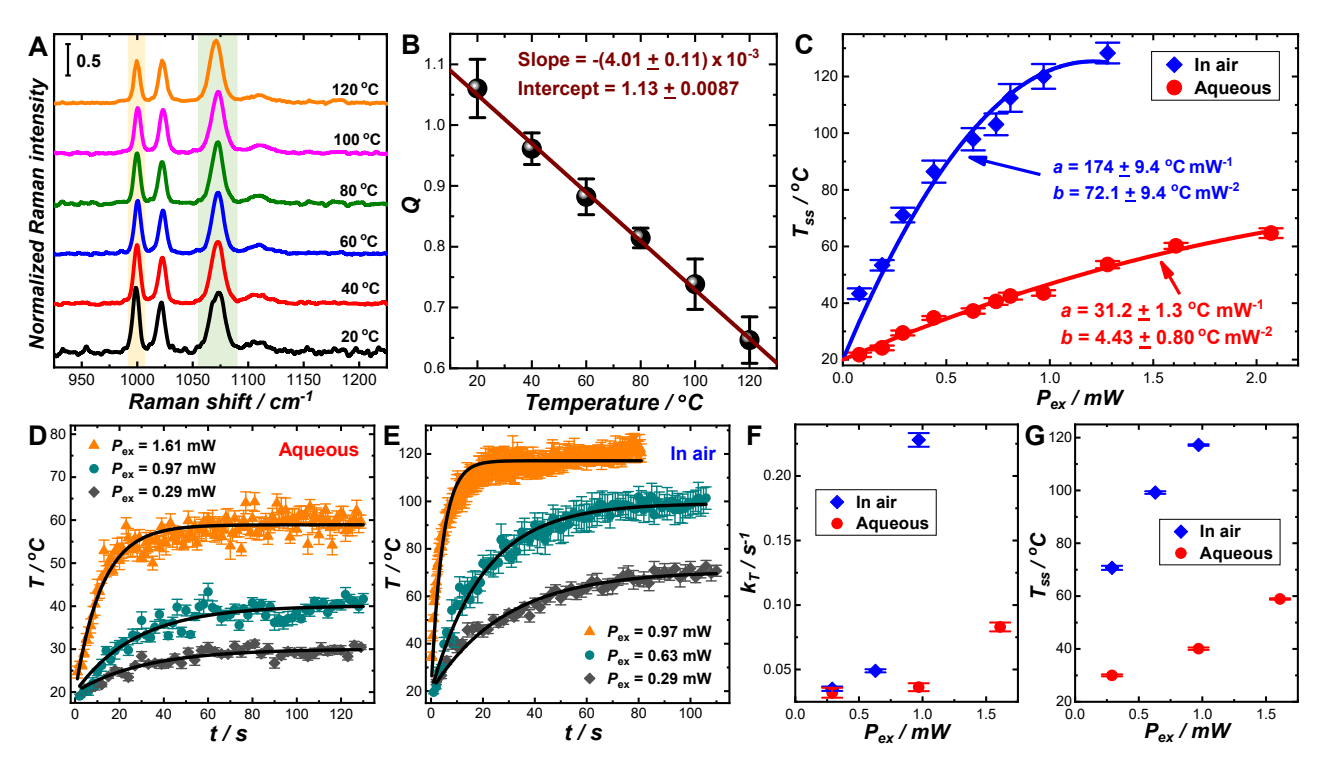


Figure 2. (A) Representative SERS spectra of TP on Ag nanoparticle arrays after the samples were maintained at various temperatures for 30 min. The intensities of the v_{CS} mode were normalized to 1 for comparison. The spectra were offset for clarity. (B) Temperature-dependence of Q. (C) P_{ex} -dependence of T_{ss} in air and in an aqueous medium. Temporal evolution of the local temperatures in the hot spots at various P_{ex} s for TP in (D) an aqueous medium and (E) in air. The curve-fitting results are shown as solid black curves in panels D and E. P_{ex} -dependence of (F) k_T and (G) T_{ss} . The error

bars in panels B-E represent the standard deviations of the SERS results collected from 10 different spots on each sample. The error bars in panels F and G represent the standard deviations associated with the least squares curve-fitting.

The difference between the thermal conductivities of water and air gave rise to significantly different local temperatures at the active sites under laser illumination, which further led to strikingly distinct kinetic profiles of the pNTP coupling reactions in atmospheric and aqueous environments. Through time-resolved SERS measurements, we monitored the reaction progress in real time by tracking the temporal evolution of the relative intensities of the v_{NN} and the $v_{CC ring}$ modes in the SERS spectra. As shown in Figure 3A and 3B, the coupling reactions proceeded at considerably faster rates and approached higher maximal yields of DMAB in air than in the aqueous medium at a P_{ex} of 0.97 mW. Although elevation of temperature seemed to kinetically boost the coupling reactions under laser illumination, no appreciable production of DMAB was observed without laser illumination even at a temperature as high as 120 °C (Figure S6 in the Supporting Information), strongly indicating that this reaction was a plasmon-driven photochemical process rather than a thermally activated catalytic reaction. We collected the time-resolved SERS results at various P_{ex} s in both atmospheric and aqueous reaction environments and the SERS-based kinetics measurements were repeated at 10 different spots on the samples under each reaction condition. We further calculated the apparent fractions of DMAB, θ , using the following equation:

$$\theta = \frac{I(1438 cm^{-1})}{I(1572 cm^{-1})Q_{DMAB}}$$
 (Equation 3),

in which $I(1438 \text{ cm}^{-1})$ is the SERS intensity of the v_{NN} mode at 1438 cm⁻¹, $I(1572 \text{ cm}^{-1})$ is the SERS intensity of the $v_{\text{CC ring}}$ mode at 1572 cm⁻¹, and Q_{DMAB} is the value of $I(1438 \text{ cm}^{-1})/I(1572 \text{ cm}^{-1})$ at 100% apparent yield of DMAB, which was achieved through plasmon-driven oxidative coupling of para-aminothiophenol on Ag nanoparticles as detailed in our previous work.²⁶ The value of Q_{DMAB}

was determined to be 2.5, as shown in Figure S7 in the Supporting Information. In all cases, the bimolecular pNTP coupling kinetics could be well-described by the following second-order rate law:

$$\theta(t) = \frac{2\theta_{max}^2 k_{obs} t}{2\theta_{max} k_{obs} t + 1}$$
 (Equation 4),

where k_{obs} is the apparent second-order rate constant and θ_{max} is the maximal θ value. The θ trajectories collected from individual spots on the samples under various reaction conditions and the curve-fitting results are shown in detail in Figures S8-S22 in the Supporting Information. To maintain the pH at 9 during the reactions, the concentration of K_2CO_3 was kept at 2 mM in the aqueous reaction medium. Switching from 2 mM K_2CO_3 to 10 μ M KOH (pH also at 9) did not introduce any noticeable modifications to the reaction rates and yields (Figure S23 in the Supporting Information).

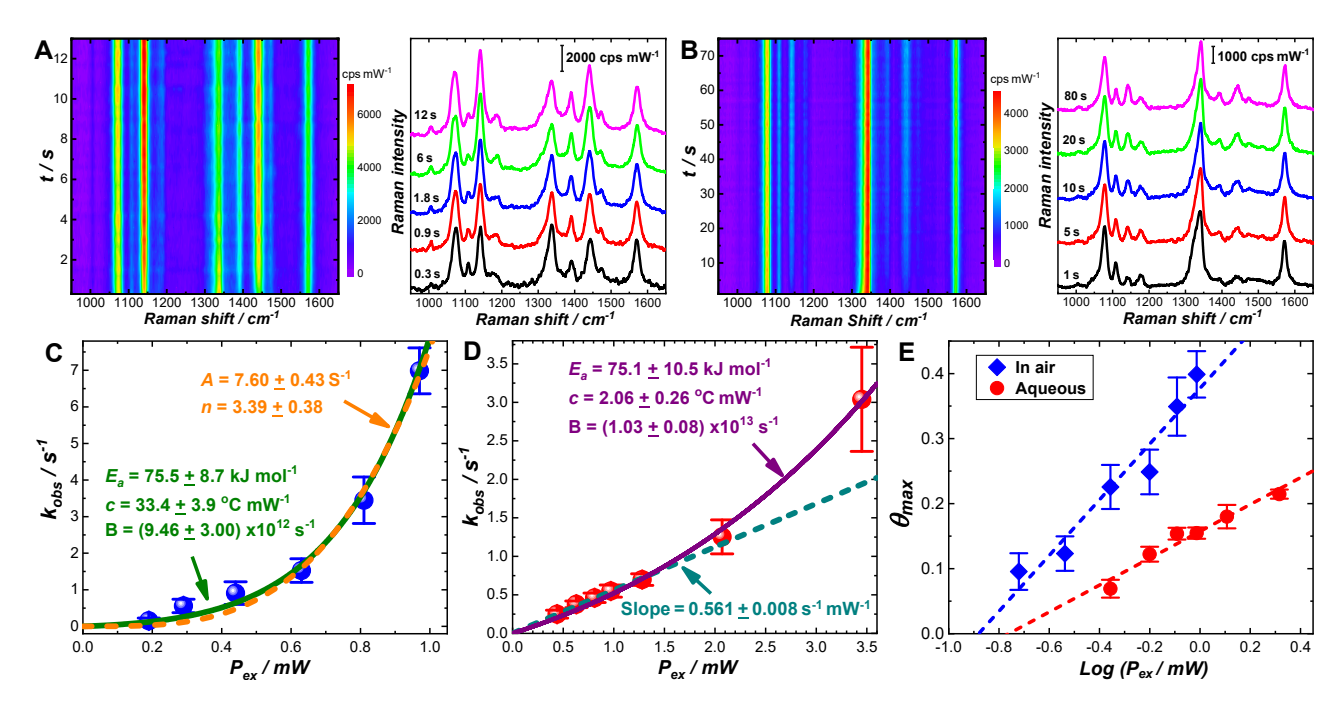


Figure 3. Representative time-resolved SERS spectra (left panels) and snapshot SERS spectra at various stages (right panels) during plasmon-driven pNTP coupling reactions in (A) air and (B) an aqueous environment at a P_{ex} of 0.97 mW. P_{ex} -dependence of k_{obs} for plasmon-driven pNTP coupling reactions in (C) air and (D) an aqueous environment. (E) P_{ex} -dependence of θ_{max} for plasmon-driven pNTP coupling reactions in atmospheric and aqueous environments. The error bars in panels C-E represent the standard deviations of the results collected from 10 different spots on the samples under each reaction condition. The curve-fitting results using various equations are shown as either solid or dash curves.

For the pNTP coupling reactions occurring in air, k_{obs} exhibited a superlinear dependence on P_{ex} in the sub-mW P_{ex} range (Figure 3C), which could be fitted with the following power function:

$$k_{obs} = A \left(\frac{P_{ex}}{1 \, mW}\right)^n \tag{Equation 5},$$

in which A is a fractional coefficient and n is an exponent, respectively. An n value of 3.39 was obtained through least-squares curve fitting (the orange dash curve in Figure 3C). Interestingly, in an aqueous reaction environment, k_{obs} became linearly proportional to P_{ex} in the range of 0.2-1.4 mW (the dark evan dash line in Figure 3D). Such strikingly different power dependence of reaction rates in different reaction media within the same P_{ex} range strongly suggested that the origin of the superlinear power dependence should not be interpreted in the context of multiphoton absorption or P_{ex} -dependent activation energy reduction for this plasmon-driven reaction under our reaction conditions. The most reasonable explanation ascribed the origin of superlinearity in power dependence to the local photothermal heating at the active sites on the Ag nanoparticle surfaces. In the aqueous environment, k_{obs} exhibited a linear dependence on P_{ex} in the low P_{ex} regime below 1.5 mW because of rather limited elevation of the local temperatures. However, when P_{ex} exceeded 1.5 mW, the superlinearity in power dependence started to develop as the photothermal effects became increasingly more significant (Figure 3D). Taking both nonthermal (linear P_{ex} -dependence) and thermal (Arrhenius relationship) contributions into considerations, we fitted the experimentally determined P_{ex} -dependence of k_{obs} using the following equation (see the olive solid curve in Figure 3C and the purple solid curve in Figure 3D):

$$k_{obs} = B\left(\frac{P_{ex}}{1 \ mW}\right) e^{-\frac{E_a}{R(273 + T_{app})}}$$
 (Equation 6),

in which B is a fractional coefficient, E_a is the activation energy associated with the rate-limiting step, R is the molar gas constant (8.314 J mol⁻¹ K⁻¹), and T_{app} is the apparent local temperature at the active sites with the unit of ${}^{\circ}$ C. Under the current reaction conditions, the pNTP coupling reactions were

sufficiently rapid, reaching the θ_{max} values far before the thermal equilibrium was established. Therefore, T_{app} during the reactions should be significantly lower than T_{ss} , and we further assumed that T_{app} depended linearly on P_{ex} by ignoring the nonlinear photothermal response term:

$$T_{app} = T_0 + cP_{ex}$$
 (Equation 7).

Here c is a photothermal transduction coefficient carrying the unit of ${}^{\circ}\text{C}$ mW⁻¹. The values of T_{app} calculated using the c values obtained from curve-fitting were considerably lower than the experimentally measured T_{ss} (Figure S24 in the Supporting Information). Strictly speaking, T_{app} should change over time during the reactions. However, further incorporating a temporally evolving T_{app} terms into Equation 6 resulted in unacceptable uncertainties in the least squares curve-fitting. Therefore, the T_{app} defined in this work should be more accurately described as the apparent local temperatures at the active sties averaged over the time duration of reactions. When switching the reaction medium from air to water, the E_a values (around 75 kJ mol⁻¹) remained essentially unchanged, whereas the value of c decreased by one order of magnitude.

The difference in local temperatures also led to significantly different maximal yields of DMAB. At identical P_{ex} s, higher θ_{max} values were achieved in air than in the aqueous environment (Figure 3E). The maximal yields of DMAB achievable under our reaction conditions were always significantly lower than 100 % because this reaction could occur only when the local field intensities exceeded certain threshold values.^{26,27} Increasing P_{ex} resulted in higher θ_{max} values as a large fraction of pNTP adsorbates became reactive. θ_{max} exhibited a linear dependence on the logarithm of P_{ex} within the P_{ex} range we investigated (Figure 3E). When extrapolating the linear dependence to zero θ_{max} , we obtained P_{ex} threshold values of 0.13 mW (corresponding to an excitation power density of 4.2 kW cm⁻²) in air and 0.19 mW (corresponding to an excitation power density of 5.9 kW cm⁻²) in aqueous environment, respectively, for this pNTP coupling reaction. The P_{ex} thresholds may vary significantly from reaction to reaction, depending on the local-field enhancements on the photocatalyst surfaces,

the chemical nature of the reactions, the excitation wavelengths, the light illumination geometries, and the local reaction environments.^{26, 28, 52, 53}

The results of the SERS-based thermometric and kinetic measurements clearly indicate that the superlinearity in the power dependence of reaction rates observed in plasmon-driven bimolecular coupling of pNTP originates primarily from photothermal heating rather than nonthermal plasmonic effects. Considering the mechanistic complexity and diversity of plasmonic photocatalysis, however, the conclusion drawn on the pNTP coupling reaction may not be universally applicable to other plasmon-driven photocatalytic reactions. Under our reaction conditions (aerobic environments and near-infrared excitations), the photoexcited hot electrons are energetically insufficient to get injected into unoccupied molecular orbitals of the pNTP adsorbates. ^{27,54} Instead, the hot electrons are injected into the antibonding π^* orbital of surface-adsorbed O₂ to produce highly reactive O₂- radicals, which further induce the rate-limiting bimolecular coupling of pNTP to produce DMAB and O₂.²⁷ As shown by our previous work,²⁷ pNTP molecules chemisorbed on Ag nanoparticle surfaces remain essentially unreactive under near-infrared excitations in an anaerobic environment. For plasmon-driven reactions whose rate-limiting steps directly involve hot carrier injection, however, it becomes possible that both multiphoton absorption and plasmon-induced activation energy reduction provide significant contributions to the superlinear power dependence of the reaction rates. Choosing Raman probes with temperature-dependent SERS features, such as TP used in this work and phenylisocyanide adsorbed to Au surfaces,⁵⁵ enables us to measure the local temperatures in the plasmonic hot spots based on the Stokes Raman shifts without the need to analyze the anti-Stokes signals that are typically several orders of magnitude weaker than the Stokes signals. In principle, the local temperatures can also be quantified based on relative intensities of anti-Stokes and Stokes SERS peaks. 45, 56-58 However, the local-field enhancements at Stokes and anti-Stokes scattering frequencies may differ drastically and the anti-Stokes-to-Stokes intensity ratios may be profoundly influenced by chemical interface damping in coupled metal-adsorbate systems, ^{57, 58} which introduce nontrivial complication to the data analysis. Integration of SERS-based kinetic measurements with straightforward SERS-based nanothermometry opens up a unique avenue to correlate the kinetics of plasmon-driven molecular transformations to the local temperatures at the active sites, representing a significant step toward quantitative understanding of thermal and nonthermal effects involved in plasmonic photocatalysis.

ASSOCIATED CONTENT

Supporting Information. Experimental details and additional figures as noted in the maintext, including a dark-field microscopy image, a light extinction spectrum, SERS spectra, and detailed kinetic results. This material is available free of charge via the Internet at http://pubs.acs.org.

AUTHOR INFORMATION

Corresponding Author

* Hui Wang – Department of Chemistry and Biochemistry, University of South Carolina, Columbia, South Carolina 29208; Email: wang344@mailbox.sc.edu; Phone: 1-803-777-2203; orcid.org/0000-0002-1874-5137.

Author

Kexun Chen – Department of Chemistry and Biochemistry, University of South Carolina, Columbia, South Carolina 29208; orcid.org/0000-0003-2809-1242.

Author Contributions

K.C. did the experiments. K.C and H.W. analyzed the data. H.W. designed the project, supervised the research, acquired funding support, and wrote the paper. Both authors have given approval to the final version of the manuscript.

Notes

The authors declare no competing financial interest.

ACKNOWLEDGMENT

This work was supported by the Macromolecular, Supramolecular, and Nanochemistry (MSN) Program in the Division of Chemistry of the National Science Foundation (NSF) under Grant CHE-2202928. K.C. was partially supported by a SPARC Award (130200-22-59284) sponsored by the University of South Carolina Office of Vice President for Research. The Zeiss Gemini500 thermal field emission scanning electron microscope used in this work was purchased using the South Carolina Science, Technology, Engineering, and Mathematics (STEM) Equipment Funds. The Hitachi HT7800 transmission electron microscope used in this work was purchased using funds provided by an NSF EPSCoR RII Track-I Award (OIA-1655740).

REFERENCES

- 1. Kale, M. J.; Avanesian, T.; Christopher, P. Direct Photocatalysis by Plasmonic Nanostructures. *ACS Catal.* **2014**, *4* (1), 116-128.
- 2. Brongersma, M. L.; Halas, N. J.; Nordlander, P. Plasmon-Induced Hot Carrier Science and Technology. *Nat. Nanotech.* **2015**, *10* (1), 25-34.
- 3. Linic, S.; Aslam, U.; Boerigter, C.; Morabito, M. Photochemical Transformations on Plasmonic Metal Nanoparticles. *Nat. Mater.* **2015,** *14* (6), 567-576.
- 4. Christopher, P.; Moskovits, M. Hot Charge Carrier Transmission from Plasmonic Nanostructures. *Annu. Rev. Phys. Chem.* **2017**, *68*, 379-398.
- 5. Zhang, Y. C.; He, S.; Guo, W. X.; Hu, Y.; Huang, J. W.; Mulcahy, J. R.; Wei, W. D. Surface-Plasmon-Driven Hot Electron Photochemistry. *Chem. Rev.* **2018**, *118* (6), 2927-2954.

- 6. Kazuma, E.; Kim, Y. Mechanistic Studies of Plasmon Chemistry on Metal Catalysts. *Angew. Chem. Inter. Ed.* **2019**, *58* (15), 4800-4808.
- 7. Cortés, E.; Besteiro, L. V.; Alabastri, A.; Baldi, A.; Tagliabue, G.; Demetriadou, A.; Narang, P. Challenges in Plasmonic Catalysis. *ACS Nano* **2020**, *14* (12), 16202-16219.
- 8. Gelle, A.; Jin, T.; de la Garza, L.; Price, G. D.; Besteiro, L. V.; Moores, A. Applications of Plasmon-Enhanced Nanocatalysis to Organic Transformations. *Chem. Rev.* **2020**, *120* (2), 986-1041.
- 9. Kherbouche, I.; Luo, Y.; Felidj, N.; Mangeney, C. Plasmon-Mediated Surface Functionalization: New Horizons for the Control of Surface Chemistry on the Nanoscale. *Chem. Mater.* **2020,** *32* (13), 5442-5454.
- 10. Devasia, D.; Das, A.; Mohan, V.; Jain, P. K. Control of Chemical Reaction Pathways by Light-Matter Coupling. *Annu. Rev. Phys. Chem.* **2021,** *72*, 423-443.
- 11. Ou, W. H.; Zhou, B. B.; Shen, J. D.; Zhao, C. H.; Li, Y. Y.; Lu, J. Plasmonic Metal Nanostructures: Concepts, Challenges and Opportunities in Photo-Mediated Chemical Transformations. *iScience* **2021**, *24* (2), 101982.
- 12. Fang, M.; Tan, X. L.; Liu, Z. X.; Hu, B. W.; Wang, X. K. Recent Progress on Metal-Enhanced Photocatalysis: A Review on the Mechanism. *Research* **2021**, *2021*, 9794329.
- 13. Zhan, C.; Liu, B. W.; Huang, Y. F.; Hu, S.; Ren, B.; Moskovits, M.; Tian, Z. Q. Disentangling Charge Carrier from Photothermal Effects in Plasmonic Metal Nanostructures. *Nat. Commun.* **2019**, *10*, 2671.
- 14. Mukherjee, S.; Libisch, F.; Large, N.; Neumann, O.; Brown, L. V.; Cheng, J.; Lassiter, J. B.; Carter, E. A.; Nordlander, P.; Halas, N. J. Hot Electrons Do the Impossible: Plasmon-Induced Dissociation of H₂ on Au. *Nano Lett.* **2013**, *13* (1), 240-247.
- 15. Zhou, L. A.; Swearer, D. F.; Zhang, C.; Robatjazi, H.; Zhao, H. Q.; Henderson, L.; Dong, L. L.; Christopher, P.; Carter, E. A.; Nordlander, P., et al. Quantifying Hot Carrier and Thermal Contributions in Plasmonic Photocatalysis. *Science* **2018**, *362* (6410), 69-72.

- 16. Baffou, G.; Bordacchini, I.; Baldi, A.; Quidant, R. Simple Experimental Procedures to Distinguish Photothermal from Hot-Carrier Processes in Plasmonics. *Light-Sci. Appl.* **2020**, *9* (1), 108.
- 17. Christopher, P.; Xin, H. L.; Marimuthu, A.; Linic, S. Singular Characteristics and Unique Chemical Bond Activation Mechanisms of Photocatalytic Reactions on Plasmonic Nanostructures.

 Nat. Mater. 2012, 11 (12), 1044-1050.
- 18. Kim, Y.; Torres, D. D.; Jain, P. K. Activation Energies of Plasmonic Catalysts. *Nano Lett.* **2016**, *16* (5), 3399-3407.
- 19. Jain, P. K. Comment on "Thermal Effects an Alternative Mechanism for Plasmon-Assisted Photocatalysis" by Y. Dubi, I. W. Un and Y. Sivan, Chem. Sci., 2020,11, 5017. *Chem. Sci.* **2020**, *11* (33), 9022-9023.
- 20. Dubi, Y.; Un, I. W.; Sivan, Y. Thermal Effects an Alternative Mechanism for Plasmon-Assisted Photocatalysis. *Chem. Sci.* **2020,** *11* (19), 5017-5027.
- 21. Sivan, Y.; Baraban, J.; Un, I. W.; Dubi, Y. Comment on "Quantifying Hot Carrier and Thermal Contributions in Plasmonic Photocatalysis". *Science* **2019**, *364* (6439), eaaw9367.
- 22. Zhou, L. A.; Swearer, D. F.; Robatjazi, H.; Alabastri, A.; Christopher, P.; Carter, E. A.; Nordlander, P.; Halas, N. J. Response to Comment on "Quantifying Hot Carrier and Thermal Contributions in Plasmonic Photocatalysis". *Science* **2019**, *364* (6439), eaaw9545.
- 23. Dubi, Y.; Un, I. W.; Sivan, Y. Reply to the 'Comment on "Thermal Effects an Alternative Mechanism for Plasmon-Assisted Photocatalysis" by P. Jain, Chem. Sci., 2020,11, Doi: 10.1039/D0sc02914a. *Chem. Sci.* **2020**, *11* (33), 9024-9025.
- 24. Zhang, X.; Li, X. Q.; Reish, M. E.; Zhang, D.; Su, N. Q.; Gutierrez, Y.; Moreno, F.; Yang, W. T.; Everitt, H. O.; Liu, J. Plasmon-Enhanced Catalysis: Distinguishing Thermal and Nonthermal Effects. *Nano Lett.* **2018**, *18* (3), 1714-1723.

- 25. Li, X. Q.; Everitt, H. O.; Liu, J. Synergy between Thermal and Nonthermal Effects in Plasmonic Photocatalysis. *Nano Res.* **2020**, *13* (5), 1268-1280.
- 26. Chen, K. X.; Wang, H. Plasmon-Driven Oxidative Coupling of Aniline-Derivative Adsorbates: A Comparative Study of Para-Ethynylaniline and Para-Mercaptoaniline. *J. Chem. Phys.* **2022**, *156* (20), 204705.
- 27. Zhang, Q. F.; Zhou, Y. D.; Fu, X. Q.; Villarreal, E.; Sun, L. C.; Zou, S. L.; Wang, H. Photothermal Effect, Local Field Dependence, and Charge Carrier Relaying Species in Plasmon-Driven Photocatalysis: A Case Study of Aerobic Nitrothiophenol Coupling Reaction. *J. Phys. Chem. C* 2019, *123* (43), 26695-26704.
- 28. Zhang, Q. F.; Chen, K. X.; Wang, H. Hot-Hole-Induced Molecular Scissoring: A Case Study of Plasmon-Driven Decarboxylation of Aromatic Carboxylates. *J. Phys. Chem. C* **2021**, *125* (38), 20958-20971.
- 29. Wang, H.; Musier-Forsyth, K.; Falk, C.; Barbara, P. F. Single-Molecule Spectroscopic Study of Dynamic Nanoscale DNA Bending Behavior of HIV-1 Nucleocapsid Protein. *J. Phys. Chem. B* **2013**, *117* (16), 4183-4196.
- 30. Aggarwal, R. L.; Farrar, L. W.; Saikin, S. K. Increase of SERS Signal Upon Heating or Exposure to a High-Intensity Laser Field: Benzenethiol on an AgFON Substrate. *J. Phys. Chem. C* **2012**, *116* (31), 16656-16659.
- 31. Sun, M. T.; Xu, H. X. A Novel Application of Plasmonics: Plasmon-Driven Surface-Catalyzed Reactions. *Small* **2012**, *8* (18), 2777-2786.
- 32. Huang, Y. F.; Zhu, H. P.; Liu, G. K.; Wu, D. Y.; Ren, B.; Tian, Z. Q. When the Signal Is Not from the Original Molecule to Be Detected: Chemical Transformation of para-Aminothiophenol on Ag During the SERS Measurement. *J. Am. Chem. Soc.* **2010**, *132* (27), 9244-9246.

- 33. van Schrojenstein Lantman, E. M.; Deckert-Gaudig, T.; Mank, A. J. G.; Deckert, V.; Weckhuysen, B. M. Catalytic Processes Monitored at the Nanoscale with Tip-Enhanced Raman Spectroscopy. *Nat. Nanotech.* **2012**, *7* (9), 583-586.
- 34. Brooks, J. L.; Frontiera, R. R. Competition between Reaction and Degradation Pathways in Plasmon-Driven Photochemistry. *J. Phys. Chem. C* **2016**, *120* (37), 20869-20876.
- 35. Zhan, C.; Chen, X. J.; Huang, Y. F.; Wu, D. Y.; Tian, Z. Q. Plasmon-Mediated Chemical Reactions on Nanostructures Unveiled by Surface-Enhanced Raman Spectroscopy. *Acc. Chem. Res.* **2019**, *52* (10), 2784-2792.
- 36. Golubev, A. A.; Khlebtsov, B. N.; Rodriguez, R. D.; Chen, Y.; Zahn, D. R. T. Plasmonic Heating Plays a Dominant Role in the Plasmon-Induced Photocatalytic Reduction of 4-Nitrobenzenethiol. *J. Phys. Chem. C* **2018**, *122* (10), 5657-5663.
- 37. Wang, C. F.; O'Callahan, B. T.; Kurouski, D.; Krayev, A.; El-Khoury, P. Z. The Prevalence of Anions at Plasmonic Nanojunctions: A Closer Look at P-Nitrothiophenol. *J. Phys. Chem. Lett.* **2020**, *11* (10), 3809-3814.
- 38. Sun, J. J.; Su, H. S.; Yue, H. L.; Huang, S. C.; Huang, T. X.; Hu, S.; Sartin, M. M.; Cheng, J.; Ren, B. Role of Adsorption Orientation in Surface Plasmon-Driven Coupling Reactions Studied by Tip-Enhanced Raman Spectroscopy. *J. Phys. Chem. Lett.* **2019**, *10* (10), 2306-2312.
- 39. Kang, L. L.; Xu, P.; Zhang, B.; Tsai, H. H.; Han, X. J.; Wang, H. L. Laser Wavelength- and Power-Dependent Plasmon-Driven Chemical Reactions Monitored Using Single Particle Surface Enhanced Raman Spectroscopy. *Chem. Commun.* **2013**, *49* (33), 3389-3391.
- 40. Kang, L. L.; Han, X. J.; Chu, J. Y.; Xiong, J.; He, X.; Wang, H. L.; Xu, P. In Situ Surface-Enhanced Raman Spectroscopy Study of Plasmon-Driven Catalytic Reactions of 4-Nitrothiophenol under a Controlled Atmosphere. *ChemCatChem* **2015**, *7* (6), 1004-1010.

- 41. Choi, H. K.; Lee, K. S.; Shin, H. H.; Kim, Z. H. Identification of the First Elementary Step in the Photocatalytic Reduction of Nitrobenzenethiols on a Metallic Surface. *J. Phys. Chem. Lett.* **2016**, 7 (20), 4099-4104.
- 42. Koopman, W.; Sarhan, R. M.; Stete, F.; Schmitt, C. N. Z.; Bargheer, M. Decoding the Kinetic Limitations of Plasmon Catalysis: The Case of 4-Nitrothiophenol Dimerization. *Nanoscale* **2020**, *12* (48), 24411-24418.
- 43. Dong, B.; Fang, Y. R.; Xia, L. X.; Xu, H. X.; Sun, M. T. Is 4-Nitrobenzenethiol Converted to p,p'-Dimercaptoazobenzene or 4-Aminothiophenol by Surface Photochemistry Reaction? *J. Raman Spectrosc.* **2011**, *42* (6), 1205-1206.
- 44. Miao, P.; Ma, Y.; Sun, M. T.; Li, J.; Xu, P. Tuning the SERS Activity and Plasmon-Driven Reduction of p-Nitrothiophenol on a Ag@MoS₂ Film. *Faraday Discussions* **2019**, *214*, 297-307.
- 45. Sarhan, R. M.; Koopman, W.; Schuetz, R.; Schmid, T.; Liebig, F.; Koetz, J.; Bargheer, M. The Importance of Plasmonic Heating for the Plasmon-Driven Photodimerization of 4-Nitrothiophenol. *Sci. Rep.* **2019**, *9*, 3060.
- 46. Dong, B.; Fang, Y. R.; Chen, X. W.; Xu, H. X.; Sun, M. T., Substrate-, Wavelength-, and Time-Dependent Plasmon-Assisted Surface Catalysis Reaction of 4-Nitrobenzenethiol Dimerizing to p,p'-Dimercaptoazobenzene on Au, Ag, and Cu Films. *Langmuir* **2011**, *27* (17), 10677-10682.
- 47. Choi, H. K.; Park, W. H.; Park, C. G.; Shin, H. H.; Lee, K. S.; Kim, Z. H. Metal-Catalyzed Chemical Reaction of Single Molecules Directly Probed by Vibrational Spectroscopy. *J. Am. Chem. Soc.* **2016**, *138* (13), 4673-4684.
- 48. Keller, E. L.; Frontiera, R. R. Ultrafast Nanoscale Raman Thermometry Proves Heating Is Not a Primary Mechanism for Plasmon-Driven Photocatalysis. *ACS Nano* **2018**, *12* (6), 5848-5855.
- 49. Cai, Z. F.; Merino, J. P.; Fang, W.; Kumar, N.; Richardson, J. O.; De Feyter, S.; Zenobi, R. Molecular-Level Insights on Reactive Arrangement in on-Surface Photocatalytic Coupling Reactions Using Tip-Enhanced Raman Spectroscopy. *J. Am. Chem. Soc.* **2022**, *144* (1), 538-546.

- 50. Rigor, J.; Kurouski, D.; Large, N., Plasonic Heating Effects in Tip-Enhanced Raman Spectroscopy (TERS). *J. Phys. Chem. C* **2022**, *126* (34), 13986-13993.
- 51. Un, I. W.; Dubi, Y.; Sivan, Y. Photothermal Nonlinearity in Plasmon-Assisted Photocatalysis. *Nanoscale* **2022**, *14* (13), 5022-5032.
- 52. Takeyasu, N.; Kagawa, R.; Sakata, K.; Kaneta, T. Laser Power Threshold of Chemical Transformation on Highly Uniform Plasmonic and Catalytic Nanosurface. *J. Phys. Chem. C* **2016**, *120* (22), 12163-12169.
- 53. Zhang, Q.; Wang, H. Mechanistic Insights on Plasmon-Driven Photocatalytic Oxidative Coupling of Thiophenol Derivatives: Evidence for Steady-State Photoactivated Oxygen. *J. Phys. Chem. C* **2018**, *122* (10), 5686-5697.
- 54. Zhao, L. B.; Zhang, M.; Huang, Y. F.; Williams, C. T.; Wu, D. Y.; Ren, B.; Tian, Z. Q. Theoretical Study of Plasmon-Enhanced Surface Catalytic Coupling Reactions of Aromatic Amines and Nitro Compounds. *J. Phys. Chem. Lett.* **2014**, *5* (7), 1259-1266.
- 55. Hu, S.; Liu, B. J.; Feng, J. M.; Zong, C.; Lin, K. Q.; Wang, X.; Wu, D. Y.; Ren, B. Quantifying Surface Temperature of Thermoplasmonic Nanostructures. *J. Am. Chem. Soc.* **2018**, *140* (42), 13686.
- 56. Xie, X.; Cahill, D. G. Thermometry of Plasmonic Nanostructures by Anti-Stokes Electronic Raman Scattering. *Appl. Phys. Lett.* **2016**, *109* (18), 183104.
- 57. Boerigter, C.; Campana, R.; Morabito, M.; Linic, S. Evidence and Implications of Direct Charge Excitation as the Dominant Mechanism in Plasmon-Mediated Photocatalysis. *Nat. Commun.* **2016,** *7*, 10545.
- 58. Boerigter, C.; Aslam, U.; Linic, S. Mechanism of Charge Transfer from Plasmonic Nanostructures to Chemically Attached Materials. *ACS Nano* **2016**, *10* (6), 6108-6115.

TOC Graphic:

